UNIVERSIDAD DE CONCEPCIÓN
FACULTAD DE CIENCIAS FÍSICAS Y MATEMÁTICAS

A PILOT SURVEY OF STAR-FORMING GALAXIES AT Z=6 WITH NOEMA

Un estudio piloto de galaxias con formación estelar a z=6 con NOEMA

By: Bárbara Paz Martínez Cuadra

Thesis presented to the Faculty of Physical Sciences and Mathematics of the University of Concepción to obtain the degree of Master in Astronomy

July 2025
Concepción, Chile

Advisor: Rodrigo Herrera-Camus

A mi familia y amigos

AGRADECIMIENTOS

En primer lugar quisiera expresar mi más puro agradecimiento a toda mi familia por su apoyo incondicional. A mis padres, quienes siempre me motivaron a seguir a pesar de las dificultades y quienes siempre han sido un ejemplo a seguir para mi. A mis hermanas, que aunque la vida nos ha mantenido físicamente distanciadas desde ya hace varios años, siempre han estado presentes de alguna u otra forma y tenerlas en mi vida ha sido crucial para seguir mi camino. A mi sobrina y hermanito, que son una constante motivación para ser mi mejor versión. Y a mis abuelos, quienes algunos ya partieron, pero siempre expresaron sus deseos de verme feliz haciendo lo que me apasiona y me gusta pensar que de algún lado me miran orgullosos.

Y mención especial a mi gatita *Alma*, mi compañera, quien estuvo presente en casi todos estos años de carrera, tanto en los desvelos y las frustraciones, como en las alegrías y celebraciones. Sin duda un pilar fundamental en todo este proceso.

Agradecer también a todas las personas que formaron parte de mi vida en estos $\sim$ 6 años en Concepción, con quienes formé amistades preciosas que valoro con la vida. Mención especial a GDMI, WOR y mis reinas. No me alcanzan las palabras para expresar mi gratitud por estas personas, por su apoyo cuando más lo necesité, por todas las risas, los juegos de cartas y un sinfín de recuerdos más. Sepan que todo lo bueno que recordaré de esta experiencia es en gran parte debido a ustedes.

Finalmente, me gustaría agradecer al Dr. Rodrigo Herrera-Camus, mi asesor de tesis, por ser de mis mayores ejemplos a seguir en esta carrera. Agradezco eternamente su confianza, su paciencia, consejos y constante motivación desde el día uno. Desde el 2019 cuando hizo su primera clase de *Astronomía II* sabía que quería trabajar con él. Espero algún día poder estar a su nivel como investigador y poder transmitir el amor por las astronomía de una forma tan pura y genuina como lo hace él.

Resumen

Presentamos observaciones del Northern Extended Millimeter Array (NOEMA) de cuatro galaxias luminosas en z $\sim$ 6, cuando el Universo tenía menos de $\sim$ 1 Gyr de antigüedad. Estas galaxias se detectan en la línea de estructura fina [CII] de 158 μm, y tres de ellas también muestran emisión continua de polvo subyacente. Las velocidades de la línea [CII] están desplazadas unos cientos de km s^{-1} con respecto a la emisión Lyα, lo que podría indicar la presencia de flujos de salida o una gran reserva de gas atómico circundante. A partir de la combinación del continuo de polvo y la emisión UV en el marco de referencia, estimamos que aproximadamente el 50 % de la formación estelar está oscurecida por el polvo, lo que concuerda con los valores encontrados en otras galaxias con formación estelar masiva en desplazamientos al rojo similares. Las relaciones de luminosidad [CII]-FIR de las galaxias detectadas por continuo son elevadas en comparación con las galaxias cercanas con luminosidades FIR similares. En un sistema, J163026+4315, la emisión de [CII] se resuelve espacialmente, lo que nos permite medir el tamaño de la fuente y el brillo superficial FIR ($\Sigma_{\rm FIR}$). Encontramos que la relación [CII]/FIR como función de $\Sigma_{\rm FIR}$ en esta fuente sigue las tendencias observadas tanto en poblaciones de galaxias locales como de alto desplazamiento al rojo. Un análisis cinemático de la emisión [CII] resuelta proporciona pruebas provisionales de la existencia de un disco giratorio, aunque se necesitan datos con mayor resolución angular para confirmarlo. Estos resultados demuestran la capacidad de NOEMA para sondear las condiciones físicas y la estructura del medio interestelar en las galaxias durante los primeros mil millones de años de la historia cósmica.

Keywords – galaxias: evolución – galaxias: alto redshift – galaxias: ISM

Abstract

We present observations from the Northern Extended Millimeter Array (NOEMA) of four luminous galaxies at $z \sim 6$, when the Universe was less than ~ 1 Gyr old. These galaxies are detected in the [CII] 158 μm fine-structure line, and three also exhibit underlying dust continuum emission. The [CII] line velocities are offset by a few hundred km s^{-1} relative to the Lyα emission, possibly indicating the presence of outflows or a large reservoir of surrounding atomic gas. From the combination of dust continuum and rest-frame UV emission, we estimate that approximately 50% of the star formation is obscured by dust, consistent with values found in other massive star-forming galaxies at similar redshifts. The [CII]-to-FIR luminosity ratios of the continuum-detected galaxies are elevated compared to nearby galaxies with similar FIR luminosities. In one system, J163026+4315, the [CII] emission is spatially resolved, allowing us to measure the source size and FIR surface brightness ($\Sigma_{\rm FIR}$). We find that the [CII]/FIR ratio as a function of $\Sigma_{\rm FIR}$ in this source follows the trends observed in both local and high-redshift galaxy populations. A kinematic analysis of the resolved [CII] emission provides tentative evidence for a rotating disk, although higher angular resolution data are needed to confirm this. These results demonstrate the power of NOEMA to probe the physical conditions and structure of the interstellar medium in galaxies in the first billion years of cosmic history.

Keywords – galaxies: evolution – galaxies: high-redshift – galaxies: ISM –

Contents

List of Tables

List of Figures

Chapter 1

Introduction

1.1 Context

Galaxies are vast gravitationally bound systems made up of stars, gas, dust, dark matter, and a supermassive black hole at their centers. A crucial component of galaxies is the interstellar medium (ISM), which corresponds to the gas and dust distributed between the stars. The ISM plays a fundamental role in galaxy evolution as the gas, which is composed mainly of hydrogen and helium, provides the raw material for star formation. This star-forming gas does not remain stationary since it is constantly flowing into, through, and out of galaxies. The cycle of exchange of gas between the galaxy and its surroundings, involving inflows of gas from the circumgalactic medium (CGM), star formation, and return of materials through stellar feedback is called the "baryon cycle". The baryon cycle maintains gas availability for galaxies and controls star formation over time. Although accretion provides fresh material, stellar winds and supernovae can heat or expel gas back into the CGM creating an active feedback relation, which governs how galaxies evolve across cosmic time.

In this context, investigations based on observations of multiple phases of the gas are required to understand the physical conditions and dynamical state of galaxies in the early Universe, which is essential to reconstruct the formation and evolution of present-day galaxies.

1.1.1 The cosmic noon

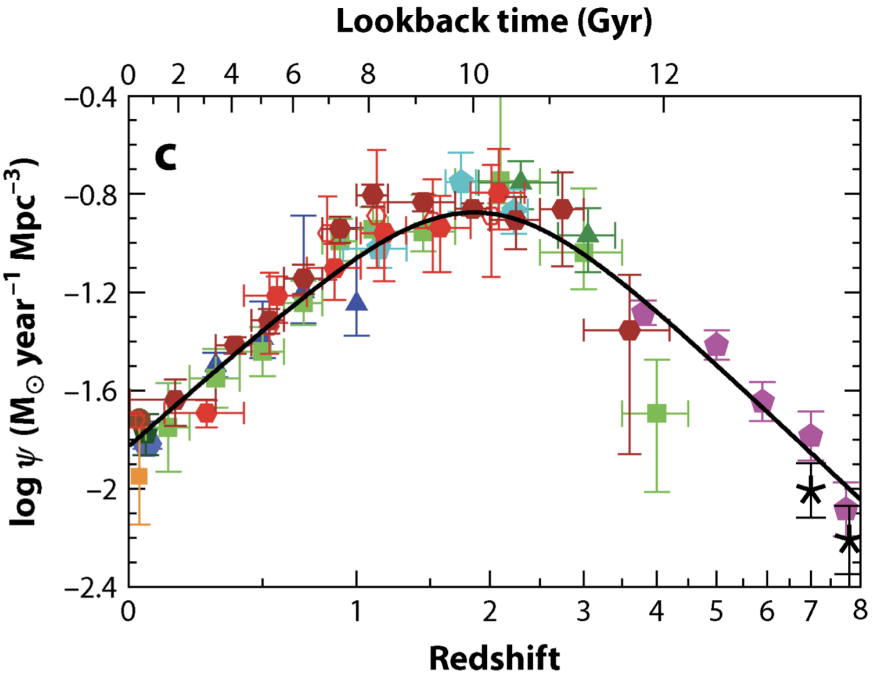

Figure 1.1.1: The cosmic star formation rate density (CSFRD) as a function of redshift. The data points indicate observations from far-ultraviolet (purple, blue and green) and infrared data (red), while the black line is the best fitting function. The star formation rate peaks around $z \sim 2$ and then decreases until the present day. Figure taken from Madau and Dickinson (2014).

By studying galaxies across different cosmic epochs, previous studies have reconstructed the evolution of the cosmic star formation rate density (CSFRD) (e.g., Lilly et al., 1996; Hopkins and Beacom, 2006; Madau and Dickinson, 2014). Figure 1.1.1 shows that the CSFRD increased over time, reaching a peak around redshift $z \sim 2$, approximately 10 billion years ago, before declining toward the present day. This peak, known as "cosmic noon", marks the most active period of star formation in the Universe.

In that sense, probing galaxy evolution before this epoch ($z > 4$) is crucial for gaining insight into the early stages of galaxy formation. However, measurements at these redshifts remain limited, with most of the available data coming from ultraviolet (UV) emission rather than from the far-infrared (FIR) dust continuum. In addition, observing cold gas in normal galaxies at high redshift, through CO lines is challenging. However, the [CII] 158 μm fine-structure line has emerged

as a powerful tracer for studying the ISM and star formation activity in early galaxies.

1.2 [CII] 158 μm transition

A valuable tracer of the ISM in distant systems like high-redshift galaxies is the [CII] 158 μm fine-structure line. As it is one of the main coolants of neutral atomic gas in the ISM (Wolfire et al., 2003), it traces different cold gas phases and is closely associated with star formation activity. This connection is because the far-ultraviolet (FUV) photons produced in star-forming regions heat the gas via the photoelectric effect on dust grains, which predominantly cools through [CII] emission (e.g., De Looze et al., 2014; Herrera-Camus et al., 2015; Schaerer et al., 2020).

As mentioned before, CO lines at high redshift are often difficult to detect in normal galaxies due to excitation and sensitivity limitations. Therefore, the [CII] line offers a more accessible alternative for probing the cold ISM in $z \gtrsim 5$ (e.g., Carilli and Walter, 2013). This is especially relevant in low-metallicity environments, where a significant fraction of the molecular gas may not be traced by CO emission—the so-called CO-faint molecular gas—which can still be detected through [CI] emission (e.g., Wolfire et al., 2010; Jameson et al., 2018). In addition, comparing its luminosity with indicators of gas heating, such as de FIR luminosity, it is possible to provide insights into the balance between heating and cooling in the ISM. (see Section 3.2.1)

1.3 Previous studies

Recent high-redshift surveys based on [CII] line and dust continuum observations have significantly expanded our understanding of cold gas in early galaxy populations.

For example, the surveys ALPINE (Le Fèvre et al., 2020; Béthermin et al., 2020; Faisst et al., 2020), REBELS (Bouwens et al., 2022), and more recently CRISTAL (Herrera-Camus et al., 2025) have contributed significantly to studying the kinematics, outflows, ISM properties, structure and sizes of normal, star-forming galaxies at $z \sim 4 - 8$ (e.g., Fujimoto et al., 2020; Ginolfi et al., 2020;

Herrera-Camus et al., 2022; Algera et al., 2023; Ikeda et al., 2024; Mitsuhashi et al., 2024; Li et al., 2024; Rowland et al., 2024; Lee et al., 2025)

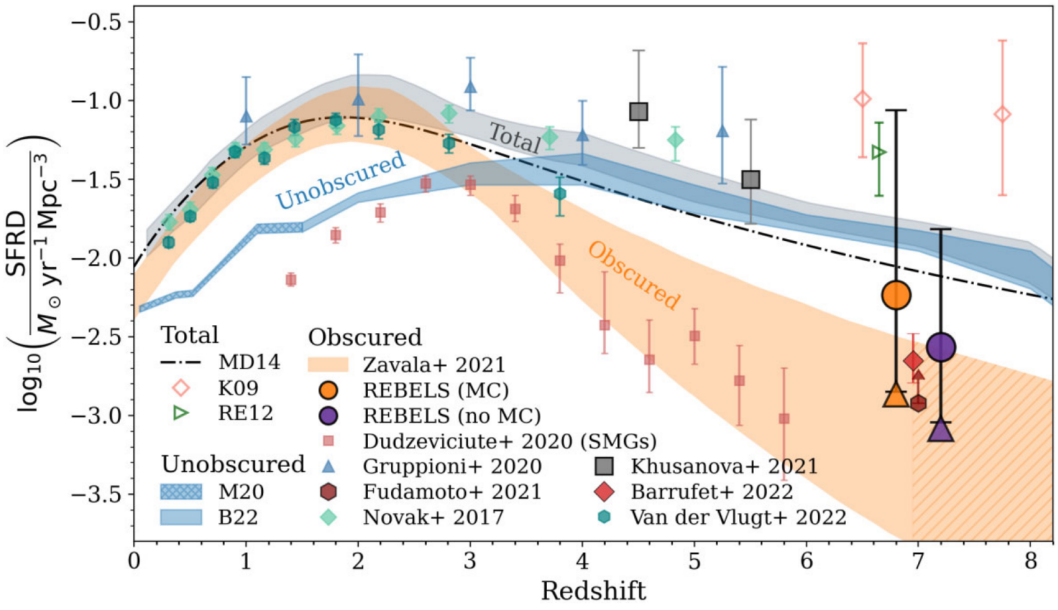

Figure 1.3.1: The cosmic star formation rate density (CSFRD) as a function of redshift. The unobscured SFRD from Moutard et al. (2020) and from Bouwens et al. (2022) are shown in blue. The dust-obscured SFRD from Zavala et al. (2021) is shown in orange, and the combined UV + IF SFRD is shown in grey. The REBELS measurements suggest a significant dust-obscured star formation already in place in the epoch of reionization. Figure taken from (Algera et al., 2023)

One of the key results from REBELS (Algera et al., 2023) is the determination of the fraction of obscured star formation in galaxies at $z \sim 6-7$. They find an average obscured fraction of 45% in their sample, indicating the presence of a large amount of dust already in place in the early Universe. These findings highlight the importance of using dust continuum observations to study galaxy evolution at early times.

In addition to dust results, several of these studies based on [CII] observations have enabled measurements of kinematics in high-redshift galaxies, which is helpful in order to answer some of the most essential questions regarding how galaxies evolve and form. From spatially resolved Hα and CO observations at "lower" redshifts ($z \leq 5$) we have learned that:

1. The level of turbulence measured by the intrinsic gas velocity dispersion in

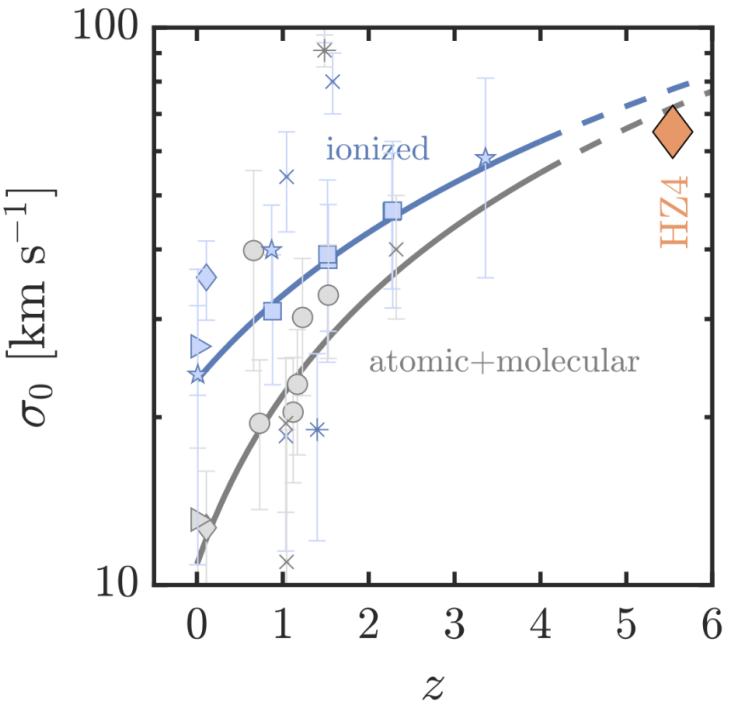

Figure 1.3.2: The evolution of the intrinsic velocity dispersion (σ_0) as a function of redshift. HZ4 ($z \sim 5.5$) is shown as an orange diamond. Values from different surveys of ionized gas are shown in blue, and from atomic and/or molecular gas are shown in gray. Figure taken from Herrera-Camus et al. (2022).

the ISM of a galaxy increases as a function of redshift (e.g., Genzel et al., 2006; Förster Schreiber et al., 2006; Stott et al., 2016; Johnson et al., 2018; Übler et al., 2019).

2. Galaxy disks are more dynamically turbulent at higher redshift (e.g., Förster Schreiber et al., 2009; Simons et al., 2017; Wisnioski et al., 2015, 2019).

More recently, spatially resolved [CII] observations have allowed similar analyses at even higher redshifts. For example, the galaxy HZ4 at $z \sim 5.5$, observed with ALMA by Herrera-Camus et al. (2022), stands out as one of the few normal star-forming galaxies at this redshift where the intrinsic velocity dispersion could be measured. As shown in Figure 1.3.2, the measured dispersion is consistent with the extrapolated trends from lower redshifts.

Moreover, HZ4 fulfills the kinematic properties described in Förster Schreiber and Wuyts (2020) of a rotating disk:

1. A smooth velocity gradient across the galaxy, defining the kinematic axis.

2. A centrally peaked velocity dispersion distribution with maximum at the position of steepest velocity gradient, defining the kinematic center.
3. Dominant rotational support, quantified by the $v_{\rm rot}/\sigma_0$ ratio.
4. Co-aligned morphological and kinematic major axes.
5. Spatial coincidence of the kinematic and morphological centers.

This makes HZ4 one of the strongest pieces of evidence to date for the presence of rotating disks at $z \sim 5.5$ when the Universe was only ~ 1 Gyr, reinforcing the importance of investigating when galaxies formed their disks in the early Universe.

1.4 NOEMA

Future progress in this field requires spatially resolved observations of both gas and dust in early galaxies. A crucial step toward enabling such high-resolution studies of ISM properties and kinematics is the identification of systems with sufficiently bright and extended [CII] and dust continuum emission.

The Northern Extended Millimeter Array (NOEMA) is one of the two observatories operated by IRAM, Europe's leading center of radio astronomy at millimeter wavelengths. Located on the Plateu de Bure in the French Alps, NOEMA consists of twelve 15-meter antennas that are mounted on tracks and can be arranged in different configurations.

As a powerful millimeter observatory in the Northern Hemisphere, NOEMA provides access to regions of the sky that are not observable from southern facilities like ALMA. The array operates using the technique of interferometry, where the signals from the multiple antennas observing the same source are combined using a supercomputer. The interferometry also uses the rotation of the Earth, this by slowly turning the antennas with respect to the cosmic source and resulting in a complete image of the object.

This capability makes NOEMA a world-class facility for studying the structure, kinematics and physical conditions of distant galaxies. With its high sensitivity and angular resolution, it is ideally suited for both the discovery and follow-up of such targets, particularly in the context of [CII] and dust continuum emission in the early Universe.

1.5 This Project

Motivated by the need of identifying systems with extended [CII] and dust continuum emission, we present NOEMA Band 3 observations of the [CII] line emission in four luminous galaxies at $z \sim 6$. These observations allow us to investigate the ISM properties and structure of typical star-forming galaxies in the early Universe, as part of a broader effort to build a representative sample at this epoch and identify the most promising candidates for future high-resolution follow-up studies of their gas kinematics.

The research is organized as follows. In Chapter 2 we present the data selection and the NOEMA observations. Chapter 3 we present the results and discussion. Finally, in Chapter 4 we summarize the main conclusions.

Chapter 2

Data Products

2.1 The sample

For this project, we searched the Subaru High-z Exploration of Low-Luminosity Quasars (SHELLQs) survey (Matsuoka et al., 2018, 2019) for systems with reliable spectroscopic redshifts and high rest-frame UV luminosities (at $\sim 1500\,\text{Å}$) — two conditions necessary for conducting NOEMA observations of the [CII] 158 μm transition, both globally and, in the future, at spatially resolved scales. We identified four luminous galaxies — J152555+4303, J151657+4228, J162833+4312, and J163026+4315 — at redshift $z \approx 6$. Two of these systems, J152555+4303 and J151657+4228, show potential evidence for AGN activity based on the width of the Lyα emission line. Galaxies J162833+4312 and J163026+4315 are also part of the Great Optically Luminous Dropout Research Using Subaru HSC (GOLDRUSH) survey (Harikane et al., 2022)

The main properties of the four galaxies are listed in Table 2.1.1, including their absolute UV magnitudes (M_{UV}), redshifts derived from the Lyα (taken from Matsuoka et al. (2018, 2019)) and [CII] emission lines, and their [CII] and

Table 2.1.1: Characteristics of the target sources.

Target	RA	Dec	$z_{\text{Ly}\alpha}$	$z_{\text{[CII]}}$	M_{UV} mag	FWHM km s^{-1}	[CII] flux Jy km s^{-1}	Cont. flux mJy	[CII]/FIR
J151657+4228	15:16:57.8	42:28:52.7	6.13	6.133	-24.35	295.46	0.71 ± 0.15	0.27 ± 0.03	1.04E-3
J152555+4303	15:25:55.7	43:03:24.0	6.27	6.277	-23.61	255.46	0.96 ± 0.13	< 0.09	–
J162833+4312	16:28:33.0	43:12:10.7	6.03	6.038	-23.20	324.03	2.2 ± 0.15	0.12 ± 0.04	3.77E-3
J163026+4315	16:30:26.3	43:15:58.1	6.02	6.033	-22.60	354.50	3.5 ± 0.15	0.52 ± 0.07	2.47E-3

dust-continuum fluxes, where the dust continuum of the galaxies was detected at rest-frame 158 μm. Figure 2.1.1 places our sample in context by showing their $M_{\rm UV}$ as a function of redshift. Compared to the ALPINE ($4 \lesssim z \lesssim 5.5$), CRISTAL ($4 \lesssim z \lesssim 6$) and REBELS ($6.5 \lesssim z \lesssim 8$) samples, our NOEMA/Band 3 observations of our targets fill an observational redshift gap between these major surveys.

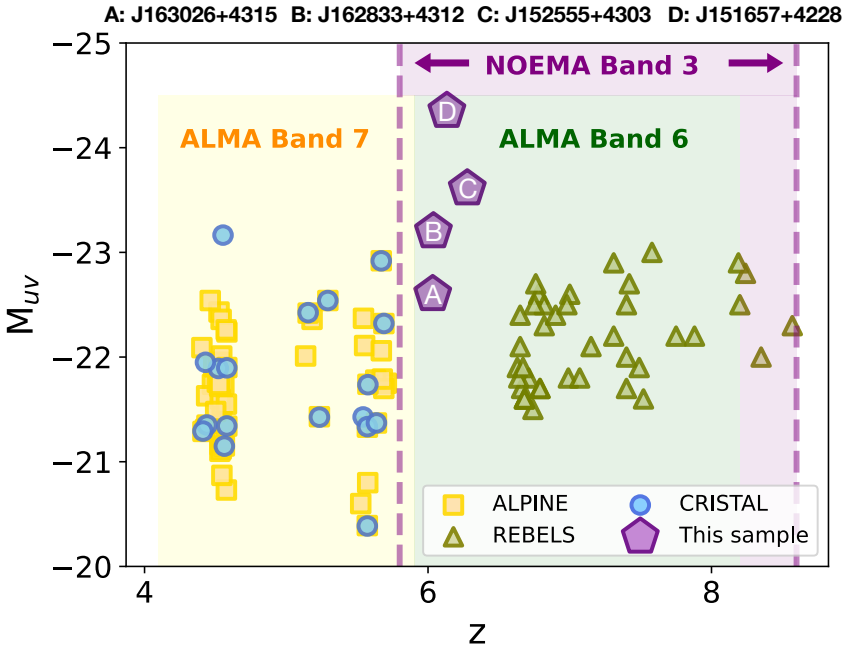

Figure 2.1.1: $M_{\rm UV}$ as a function of redshift. The purple markers show the four galaxies in our sample. For comparison, we include galaxies from the ALPINE survey (Cassata et al., 2020), the REBELS survey (Bouwens et al., 2022), and from the CRISTAL survey (Herrera-Camus et al., 2025). Colored bars indicate the bandpasses used in each survey, illustrating their corresponding redshift ranges. Some REBELS sources appear outside the redshift range of Band 6 due to observations carried out targeting other ISM tracers (e.g., the $[\rm OIII]_{88\mu m}$ transition).

2.2 Observations

We used the NOEMA interferometer in its most compact configuration (D) and Band 3 ($\nu_{\rm sky} = 196.128 - 276.000$ GHz) to observe the [CII] 158 µm fine-structure line and underlying dust continuum. The first two targets, J162833+4312 and J163026+4315, were observed on April 6 and 10, 2023, with a total on-source integration time of 19.24 hours for both. For these galaxies, the [CII]

Table 2.2.1: Summary of the NOEMA observations properties

Target	Beam Size	Line Channel RMS mJy beam^{-1}	Cont. RMS Jy beam^{-1}
J151657+4228	0.62" × 0.75"	0.69	3.7E-5
J152555+4303	0.64" × 0.75"	0.55	3.3E-5
J162833+4312	0.60" × 0.75"	0.75	3.9E-5
J163026+4315	0.60" × 0.76"	0.76	3.6E-5

line is redshifted to observed frequencies of $\nu_{\rm obs} = 270.322\,$GHz and 270.511 GHz, respectively. The remaining two galaxies, J152555+4303 and J151657+4228, were observed from April 8 to 9, 2023, with a total on-source time of 10.34 hours for both sources. Their [CII] lines are redshifted to $\nu_{\rm obs} = 261.475\,$GHz and $\nu_{\rm obs} = 266.785\,$GHz, respectively.

Data reduction was carried out using the Grenoble Image and Line Data Analysis Software (GILDAS) developed by IRAM (Guilloteau and Lucas, 2000), specifically employing the `CLIC` and `MAPPING` packages. The resulting synthesized beams have an average size of $\theta_{\rm beam} \approx 0.62" \times 0.75"$, corresponding to a physical scale of $\sim 4.5\,$kpc at $z = 6$. The achieved sensitivities range from 0.55 to 0.76 mJy beam^{-1} for the cube (measured in 40 km s^{-1} channels), and from 36 to 39 μJy beam^{-1} for the continuum maps. A detailed summary of the synthesized beam sizes and noise levels is provided in Table 2.2.1.

Chapter 3

Results

3.1 [CII] line and dust continuum detections

We detect all four galaxies in the [CII] 158 μm line emission with signal-to-noise ratios of $S/N \gtrsim 2.5$. Three of them are also detected in the dust continuum, with the exception of J152555+4303, which shows no significant continuum emission. This is notable given that all four galaxies have comparable star formation rates (SFR) and were observed to similar depths. The estimated values of the star formation rates based on the UV and IF are listed in 3.1.1, following Wuyts et al. (2008) for the UV-based SFR and Murphy et al. (2011) for the FIR-based SFR.

Table 3.1.1: Estimated values of star formation rate based on the UV and IR.

Target	$\mathrm{SFR_{UV}}$ ($\mathrm{M_\odot\ yr^{-1}}$)	$\mathrm{SFR_{FIR}}$ ($\mathrm{M_\odot\ yr^{-1}}$)	f_{obs}
J151657+4228	194	133	0.40
J152555+4303	77	–	–
J162833+4312	77	69	0.47
J163026+4315	44	307	0.84

We derived the total far-infrared (FIR; 8–1000 μm) luminosity from the NOEMA Band 3 continuum by assuming a modified blackbody with a dust temperature of $T_{\mathrm{dust}} = 45$ K and a dust emissivity index of $\beta = 1.8$, following Béthermin et al. (2020). The obscured fraction of star formation, f_{obs}, was estimated as the ratio between the dust-obscured star formation—traced by the rest-frame FIR continuum—and the total star formation rate (SFR), which includes both obscured

and unobscured components. Specifically, we measure $f_{\rm obs} = {\rm SFR_{IR}}/({\rm SFR_{IR}} + {\rm SFR_{UV}})$. For the three systems in our sample with dust continuum detections, we find that $f_{\rm obs}$ varies from $\sim 40 - 80\%$ (see Table 3.1.1), consistent with previous studies of massive star-forming galaxies at similar redshifts (e.g., Fudamoto et al., 2020; Algera et al., 2023; Mitsuhashi et al., 2024).

The left column of Figure 3.1.1 shows the global [CII] spectra for each galaxy, extracted within a circular aperture of 1" radius (∼6 kpc). The best-fit single Gaussian profiles are overplotted. Dashed lines mark the expected velocity of the Lyα lines based on redshifts from Matsuoka et al. (2018, 2019). The comparison between the [CII] and Lyα lines confirms the significance of the [CII] line detections and reveals velocity offsets between the two lines (see Section 3.3).

The middle column of Figure 3.1.1 presents the [CII] integrated intensity maps. These were obtained by integrating the emission over a velocity range of approximately ±250 km s^{-1}, corresponding to the orange-filled regions shown in the spectra. The right column of Figure 3.1.1 displays the dust continuum maps. As noted, J152555+4303 shows no detectable continuum emission at the sensitivity of our observations. The measured [CII] line and continuum flux densities $S_{\rm cont}$ are reported in Table 2.1.1.

Interestingly, for J163026+4315, both the [CII] and dust continuum maps show emission that extends beyond the beam size, with an effective radii of $R_e \approx 0.8$", which corresponds to ≈ 4.6 kpc at the redshift of the source. This is a factor of ~ 2 larger than the average size of massive star-forming galaxies at $z \sim 6$ (Fudamoto et al., 2020). One possibility is that J163026+4315 is a merger between two or more systems that remain unresolved in our current observations.

Given the bright and extended nature of J163026+4315, we recently conducted deep follow up NOEMA Band 3 observations (∼ 35 hr) using the extended array configuration (Program ID W23DA, PI Förster Schreiber). The analysis of these data will be presented in a forthcoming paper.

3.2 The [CII]/FIR luminosity ratio

The [CII] line is one of the main coolants of neutral atomic gas (Wolfire et al., 2003). Comparing its luminosity with indicators of gas heating, such as the

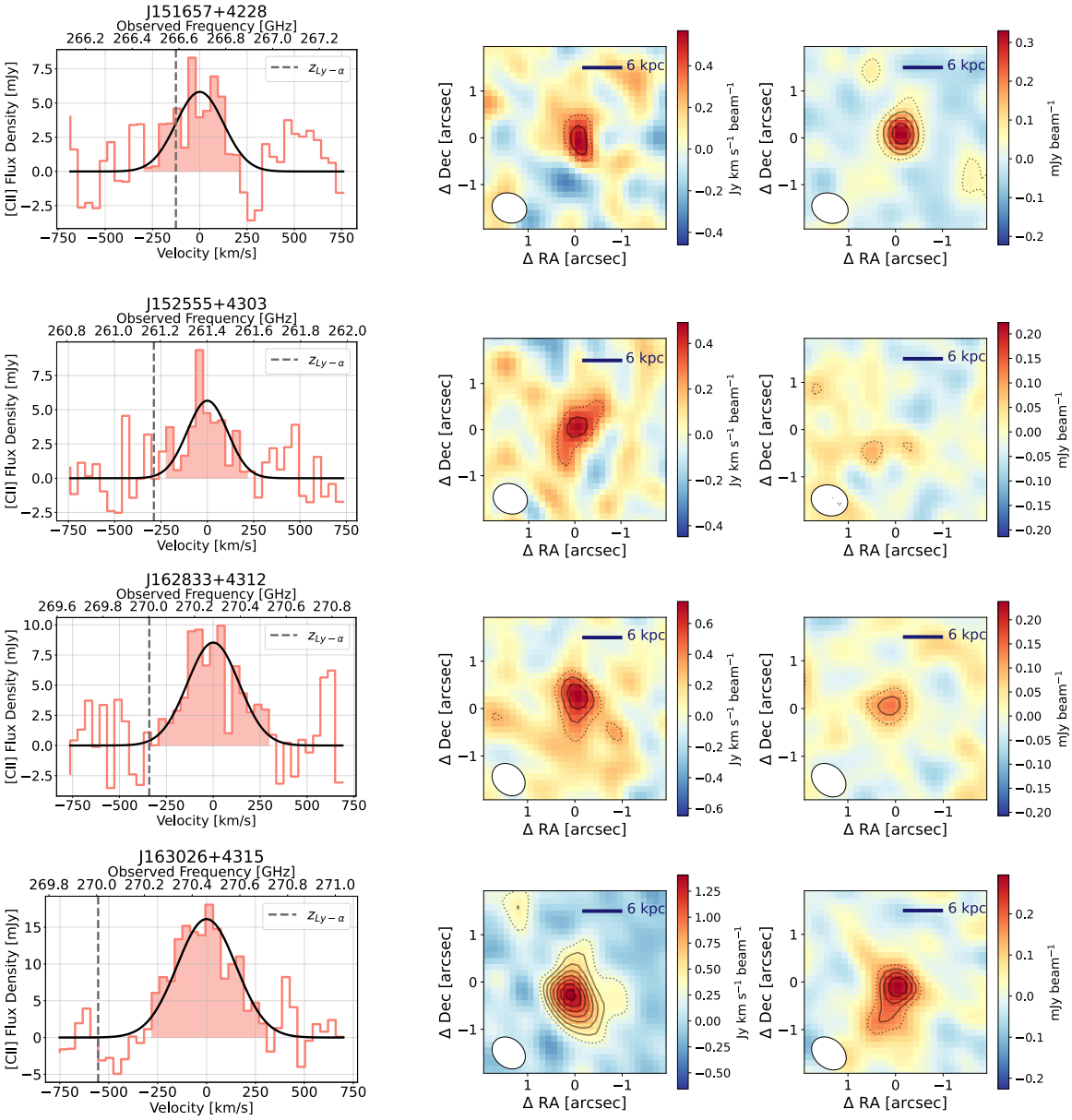

Figure 3.1.1: (*Left*) [CII] 158 μm spectrum of each galaxy, extracted inside a circular aperture of 1" radius. (*Center*) Integrated intensity map of each galaxy. The contours show a 2σ detection (dotted line) and then increase up to 9σ (solid lines), in steps of 1σ. (*Right*) Dust continuum emission, the contours start at 2σ (dotted line) and then increase up to 5σ (solid lines), also in steps of 1σ . The beam size is shown in the bottom-left corner of both integrated intensity and continuum map. J152555+4304 was not detected in the continuum.

far-infrared (FIR) luminosity, allows us to study the heating and cooling balance of the interstellar medium (ISM). The [CII]/FIR ratio is therefore linked to the physical conditions of the ISM, and it tends to decrease around $L_{\rm FIR} \sim 10^{11}\,L_{\odot}$, as shown in Figure 3.2.1. This decrease, known as the [CII] line deficit (e.g., Malhotra et al., 2001; Smith et al., 2017; Herrera-Camus et al., 2018a), may arise from several mechanisms: the destruction or charging of dust grains in strong radiation fields (e.g., Kaufman et al., 1999; Malhotra et al., 2001; Díaz-Santos et al., 2017), high ionization parameters in dusty H II regions (e.g., Graciá-Carpio et al., 2011; Herrera-Camus et al., 2018b), the influence of AGN on the ionization state of the gas (e.g., Langer and Pineda, 2015; Herrera-Camus et al., 2018b), the saturation of [CII] line emission in dense photodissociation regions (PDRs) where densities exceed the line critical density (Herrera-Camus et al., 2018b; Bisbas et al., 2022).

The [CII]/FIR values of the three galaxies in our sample with dust continuum detections are show in Figure 3.2.1, and listed in Table 2.1.1. The error bars indicate how the ratio would vary if different dust temperatures in the range 40 K $\lesssim T_{\rm dust} \lesssim$ 60 K were assumed. For comparison, we include measurements from nearby galaxies (Lutz et al., 2016; Spilker et al., 2016; Herrera-Camus et al., 2018a), and star-forming galaxies at $3 \lesssim z \lesssim 6$ (Spilker et al., 2016; Béthermin et al., 2020).

The galaxies in our sample follow the general trend, with two of them exhibiting higher [CII]/FIR ratios for a given $L_{\rm FIR}$ than nearby galaxies. This has been interpreted as consequence of high-z galaxies being more gas-rich (e.g., Narayanan and Krumholz, 2017; Herrera-Camus et al., 2025).

The right panel of Figure 3.2.1 shows the [CII]/FIR line ratio as a function of the FIR surface brightness, $\Sigma_{\rm FIR}$. The [CII]/FIR$-\Sigma_{\rm FIR}$ scaling relation derived for main-sequence star-forming at $z \gtrsim 3$ by Herrera-Camus et al. (2025) is shown as a gray line. The correlation between [CII]/FIR and $\Sigma_{\rm FIR}$ is tighter than with $L_{\rm FIR}$ (e.g., Lutz et al., 2016; Díaz-Santos et al., 2017; Herrera-Camus et al., 2018a), likely because $\Sigma_{\rm FIR}$ more directly traces the ratio of the FUV radiation field intensity (G_0) to the neutral gas density ($n_{\rm H}$), both of which are key parameters regulating [CII] emission. We observe that for J163026+4315 — the system with extended [CII] and dust continuum emission, and for which a source size can be measured — the data point no longer appears offset from the general relation for

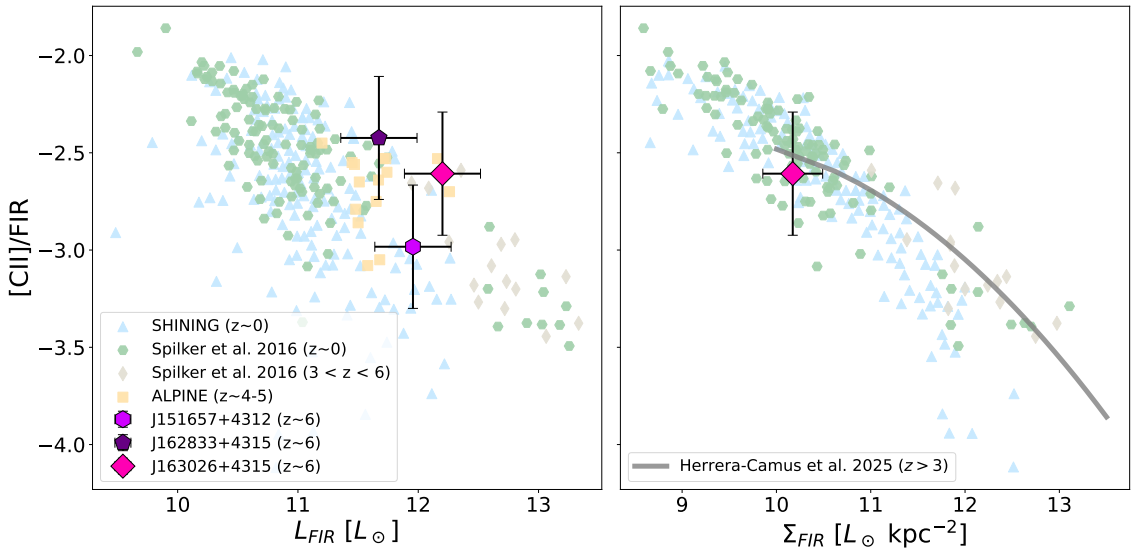

Figure 3.2.1: [CII]/FIR ratio as a function of the FIR luminosity (left) for the three galaxies detected in the dust continuum, and as a function of $\Sigma_{\rm FIR}$ (*right*) for the one extended galaxy where the size can be measured. For comparison, we show galaxies from the SHINING survey (z∼0) (Lutz et al., 2016), galaxies at $z \sim 0$ and $3 < z < 6$ from Spilker et al. (2016), from the ALPINE survey (z $\sim$ 4-6; Béthermin et al., 2020), and a scaling relation for $z \gtrsim 3$ main-sequence star-forming galaxies from Herrera-Camus et al. (2025).

star-forming galaxies at $z \approx 0$, but instead follows the overall trend.

3.3 Comparison between the Lyα and [CII] transitions

Lyα is a resonant line, which often results in a velocity offset relative to non-resonant lines (e.g., Steidel et al., 2010; Erb et al., 2014; Hashimoto et al., 2015; Cassata et al., 2020). Such an offset with respect to the [CII] line may arise from, for example, the presence of a large reservoir of atomic gas surrounding the galaxy (e.g., Erb et al., 2014), or from gas being expelled in outflows (e.g., Verhamme et al., 2006).

Figure 3.3.1 shows the Lyα–[CII] velocity offset for the galaxies in our sample, using Lyα measurements from (Matsuoka et al., 2018, 2019). The left panel presents the velocity offset as a function of the Lyα equivalent width (EW$_0$(Lyα)), and the right panel as a function of the absolute UV magnitude ($M_{\rm UV}$). For

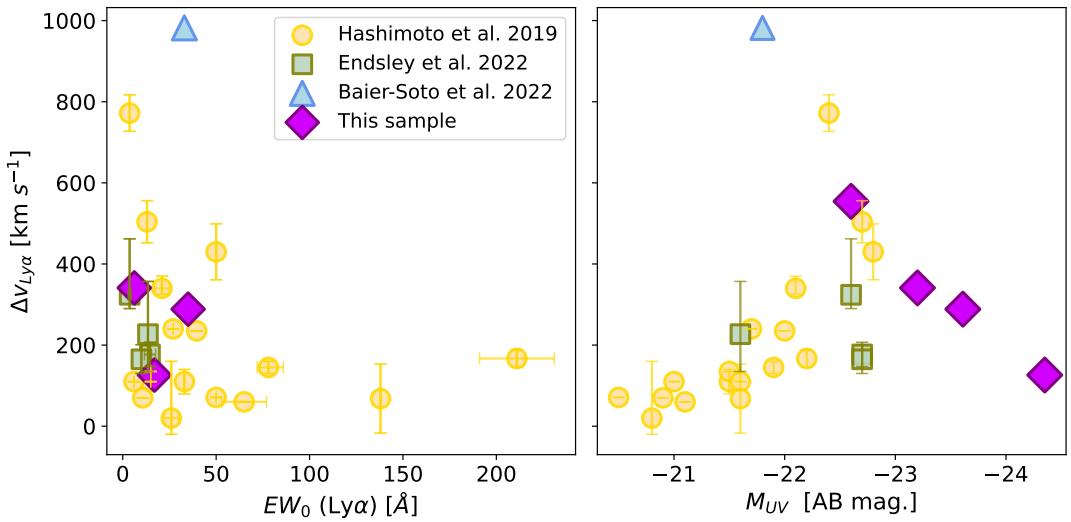

Figure 3.3.1: Velocity offset between Lyα and [CII] emission lines as a function of Lyα equivalent width (*left*) and the absolute UV magnitude (*right*). We include galaxies from Hashimoto et al. (2019) ($6 \lesssim z \lesssim 8$), Endsley et al. (2022) ($6.6 \lesssim z \lesssim 7$), and Baier-Soto et al. (2022) ($z = 7.2$) for comparison. The galaxies of this sample are shown in both panels in purple.

comparison, we include observations of high-redshift star-forming galaxies from Hashimoto et al. (2019), Endsley et al. (2022), and Baier-Soto et al. (2022).The galaxies in our sample at $z \sim 6$ show Lyα–[CII] velocity offsets in the range $\sim 200 - 500$ km s^{-1}, comparable to those reported in these previous studies.

The observed trend of the Lyα–[CII] velocity offset as a function of EW$_0$(Lyα) and $M_{\rm UV}$ can be interpreted as reflecting either larger column densities of atomic gas or outflows driven by intense star formation, respectively. We find that our systems are consistent with the trend observed as a function of EW$_0$(Lyα), which is low for our galaxies. On the other hand, the Lyα–[CII]velocity offsets tend to be small relative to the expectations from the increasing velocity offset with UV luminosity observed in other high-redshift systems. Adopting the relation $\Delta v_{\rm Ly\alpha} \sim 2 \times v_{\rm out}$ (e.g., Verhamme et al., 2006), the measured velocity offsets imply potential outflow velocities in the range of $\sim$ 100–300 km s^{-1}.

3.4 Kinematic analysis of J163026+4315

The [CII] line emission in J163026+4315 extends beyond the NOEMA synthesized beam, enabling a kinematic analysis of the system. To this end, we constructed

the velocity map (moment 1) by calculating the intensity-weighted mean velocity along the spectral axis, and the velocity dispersion map (moment 2) by computing the square root of the intensity-weighted second central moment of the velocity distribution.

Figure 3.4.1 shows the velocity field (left), the velocity dispersion map (center), and the rotation curve (right) of the galaxy. The kinematic center, and the kinematic axis were chose to coincide with the region where velocity dispersion peak and to maximize the velocity gradient and spatial coverage of the [CII]line emission. This yielded a PA_{kin} of 9° east of north. For comparison, the red dashed line in Figure 3.4.1 indicates the morphological major axis (PA_{morph} = 18° east of north), and the red cross marks the morphological center, both derived from a two-dimensional Gaussian fit to the [CII] line integrated intensity map. We find that the morphological and kinematic major axes are broadly aligned, and the kinematic and morphological centers are spatially coincident within the size of the beam.

To measure the rotation curve, we placed circular apertures with a 0.4" radius (comparable to the beam size) along the major kinematic axis, spaced by 0.25". Within each aperture, we measured the central velocity to trace the rotation curve. The rotation curve and the velocity field reveal a gradient from north to south, and the dispersion map shows a centrally peaked velocity dispersion. Altogether, these kinematic characteristics, along with the alignment between the kinematic and morphological center and axes, hints the presence of a rotating disk in J163026+4315, following the criteria described in Förster Schreiber and Wuyts (2020), although the possibility of a merger cannot be excluded with the current data, particularly considering that merging activity is common among galaxies at these early epochs. Upcoming high angular resolution observations with NOEMA will help clarify this scenario.

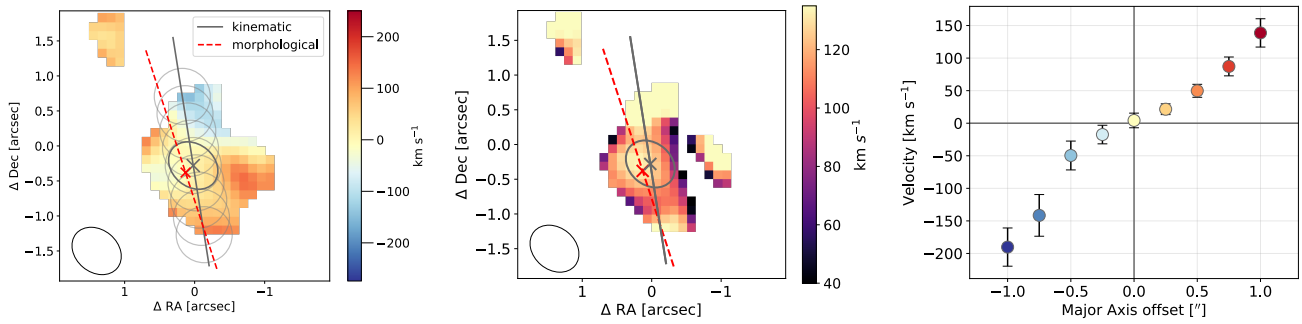

Figure 3.4.1: J163026+4315 [CII] velocity field (*left*), velocity dispersion map (*center*) and rotation curve (*right*). The synthesized beam ($\theta = 0.60$" $\times$ 0.76") is shown in the bottom-left corner of both maps. The gray solid line represents the major kinematic axis with a PA $= 9^{\text{o}}$, where the kinematic center is inside the gray beam-size region at the center. The [CII] morphological major axis is represented with the red dashed line, with the peak of [CII] shown with a red cross.

Chapter 4

Conclusions

In this study, we present results from a NOEMA Band 3 pilot program targeting four luminous galaxies at $z \sim 6$.

The main results are summarized as follows:

1. All four galaxies were detected in [CII] line emission, and three of them were also detected in the dust continuum (see Fig. 3.1.1).

2. From the rest-frame UV and dust continuum emission, we measure obscured star-formation fractions in the $f_{\rm obs} \sim 0.5 - 0.8$ range, comparable to what has been observed in other massive star-forming galaxies at $z \gtrsim 4$ (Fudamoto et al., 2020; Mitsuhashi et al., 2024; Algera et al., 2023).

3. We measure [CII]/FIR ratios that are consistent with those of typical star-forming galaxies at $z \gtrsim 4$ (e.g., Spilker et al., 2016; Herrera-Camus et al., 2025), but elevated compared to local galaxies with similar $L_{\rm FIR}$ (e.g., Herrera-Camus et al., 2018a; Lutz et al., 2016), as expected if the high-z systems are more gas rich (e.g., Narayanan and Krumholz, 2017). For the spatially resolved system J163026+4315, we also examine the [CII]/FIR ratio as a function of $\Sigma_{\rm FIR}$, which follows the tighter correlation observed in both nearby and high-redshift systems (e.g., Lutz et al., 2016; Herrera-Camus et al., 2018a, 2025).

4. We observe velocity offsets between the Lyα and [CII] lines in the range of $\sim$ 200–500 $\mathrm{km\,s^{-1}}$, consistent with values observed in other high-redshift systems (Baier-Soto et al., 2022; Hashimoto et al., 2019; Endsley et al., 2022),

and with the low $EW_0(Ly\alpha)$ and/or high M_{UV} measured in our sources.

5. The spatially extended [CII] emission detected in J163026+4315 allows us to study its kinematics. We observe a north–south velocity gradient and a centrally peaked velocity dispersion. The rough alignment between the kinematic and morphological centers and axes provide tentative evidence that this galaxy may already host a rotating disk. Future NOEMA high-angular resolution observations will help confirm this interpretation.

Our study highlights the potential of NOEMA to probe the physical conditions and dynamical states of early galaxies, offering valuable insights into their formation and evolution. An important next step is to identify additional targets in the Northern hemisphere and increase the number of high-resolution observations of both gas and dust. This will be essential for studying the physical processes that govern galaxy evolution in the early Universe.

References

Algera, H. S. B., Inami, H., Oesch, P. A., Sommovigo, L., Bouwens, R. J., Topping, M. W., Schouws, S., Stefanon, M., Stark, D. P., Aravena, M., Barrufet, L., da Cunha, E., Dayal, P., Endsley, R., Ferrara, A., Fudamoto, Y., Gonzalez, V., Graziani, L., Hodge, J. A., Hygate, A. P. S., de Looze, I., Nanayakkara, T., Schneider, R., and van der Werf, P. P. (2023). The ALMA REBELS survey: the dust-obscured cosmic star formation rate density at redshift 7. *MNRAS*, 518(4):6142–6157.

Baier-Soto, R., Herrera-Camus, R., Förster Schreiber, N. M., Contursi, A., Genzel, R., Lutz, D., and Tacconi, L. (2022). A tentative $\sim$1000 km s^{-1} offset between the [CII] 158 m and Lyα line emission in a star-forming galaxy at z = 7.2. *A&A*, 664:L5.

Béthermin, M., Fudamoto, Y., Ginolfi, M., Loiacono, F., Khusanova, Y., Capak, P. L., Cassata, P., Faisst, A., Le Fèvre, O., Schaerer, D., Silverman, J. D., Yan, L., Amorin, R., Bardelli, S., Boquien, M., Cimatti, A., Davidzon, I., Dessauges-Zavadsky, M., Fujimoto, S., Gruppioni, C., Hathi, N. P., Ibar, E., Jones, G. C., Koekemoer, A. M., Lagache, G., Lemaux, B. C., Moreau, C., Oesch, P. A., Pozzi, F., Riechers, D. A., Talia, M., Toft, S., Vallini, L., Vergani, D., Zamorani, G., and Zucca, E. (2020). The ALPINE-ALMA [CII] survey: Data processing, catalogs, and statistical source properties. *A&A*, 643:A2.

Bisbas, T. G., Walch, S., Naab, T., Lahén, N., Herrera-Camus, R., Steinwandel, U. P., Fotopoulou, C. M., Hu, C.-Y., and Johansson, P. H. (2022). The Origin of the [C II] Deficit in a Simulated Dwarf Galaxy Merger-driven Starburst. *ApJ*, 934(2):115.

Bouwens, R. J., Smit, R., Schouws, S., Stefanon, M., Bowler, R., Endsley, R., Gonzalez, V., Inami, H., Stark, D., Oesch, P., Hodge, J., Aravena, M., da Cunha, E., Dayal, P., de Looze, I., Ferrara, A., Fudamoto, Y., Graziani, L., Li, C., Nanayakkara, T., Pallottini, A., Schneider, R., Sommovigo, L., Topping, M., van der Werf, P., Algera, H., Barrufet, L., Hygate, A., Labbé, I., Riechers, D., and Witstok, J. (2022). Reionization Era Bright Emission Line Survey: Selection and Characterization of Luminous Interstellar Medium Reservoirs in the z $>$ 6.5 Universe. *ApJ*, 931(2):160.

Carilli, C. L. and Walter, F. (2013). Cool Gas in High-Redshift Galaxies. *ARA&A*, 51(1):105–161.

Cassata, P., Morselli, L., Faisst, A., Ginolfi, M., Béthermin, M., Capak, P., Le Fèvre, O., Schaerer, D., Silverman, J., Yan, L., Lemaux, B. C., Romano, M., Talia, M., Bardelli, S., Boquien, M., Cimatti, A., Dessauges-Zavadsky, M., Fudamoto, Y., Fujimoto, S., Giavalisco, M., Hathi, N. P., Ibar, E., Jones, G., Koekemoer, A. M., Méndez-Hernandez, H., Mancini, C., Oesch, P. A., Pozzi, F., Riechers, D. A., Rodighiero, G., Vergani, D., Zamorani, G., and Zucca, E. (2020). The ALPINE-ALMA [CII] survey. Small Lyα-[CII] velocity offsets in main-sequence galaxies at $4.4 < z < 6$. *A&A*, 643:A6.

De Looze, I., Cormier, D., Lebouteiller, V., Madden, S., Baes, M., Bendo, G. J., Boquien, M., Boselli, A., Clements, D. L., Cortese, L., Cooray, A., Galametz, M., Galliano, F., Graciá-Carpio, J., Isaak, K., Karczewski, O. Ł., Parkin, T. J., Pellegrini, E. W., Rémy-Ruyer, A., Spinoglio, L., Smith, M. W. L., and Sturm, E. (2014). The applicability of far-infrared fine-structure lines as star formation rate tracers over wide ranges of metallicities and galaxy types. *A&A*, 568:A62.

Díaz-Santos, T., Armus, L., Charmandaris, V., Lu, N., Stierwalt, S., Stacey, G., Malhotra, S., van der Werf, P. P., Howell, J. H., Privon, G. C., Mazzarella, J. M., Goldsmith, P. F., Murphy, E. J., Barcos-Muñoz, L., Linden, S. T., Inami, H., Larson, K. L., Evans, A. S., Appleton, P., Iwasawa, K., Lord, S., Sanders, D. B., and Surace, J. A. (2017). A Herschel/PACS Far-infrared Line Emission Survey of Local Luminous Infrared Galaxies. *ApJ*, 846(1):32.

Endsley, R., Stark, D. P., Bouwens, R. J., Schouws, S., Smit, R., Stefanon, M., Inami, H., Bowler, R. A. A., Oesch, P., Gonzalez, V., Aravena, M., da Cunha, E., Dayal, P., Ferrara, A., Graziani, L., Nanayakkara, T., Pallottini, A., Schneider, R., Sommovigo, L., Topping, M., van der Werf, P., and Hutter, A. (2022). The REBELS ALMA Survey: efficient Ly α transmission of UV-bright z 7 galaxies from large velocity offsets and broad line widths. *MNRAS*, 517(4):5642–5659.

Erb, D. K., Steidel, C. C., Trainor, R. F., Bogosavljević, M., Shapley, A. E., Nestor, D. B., Kulas, K. R., Law, D. R., Strom, A. L., Rudie, G. C., Reddy, N. A., Pettini, M., Konidaris, N. P., Mace, G., Matthews, K., and McLean, I. S. (2014). The Lyα Properties of Faint Galaxies at z ~2-3 with Systemic Redshifts and Velocity Dispersions from Keck-MOSFIRE. *ApJ*, 795(1):33.

Faisst, A. L., Schaerer, D., Lemaux, B. C., Oesch, P. A., Fudamoto, Y., Cassata, P., Béthermin, M., Capak, P. L., Le Fèvre, O., Silverman, J. D., Yan, L., Ginolfi, M., Koekemoer, A. M., Morselli, L., Amorín, R., Bardelli, S., Boquien, M., Brammer, G., Cimatti, A., Dessauges-Zavadsky, M., Fujimoto, S., Gruppioni, C., Hathi, N. P., Hemmati, S., Ibar, E., Jones, G. C., Khusanova, Y., Loiacono, F., Pozzi, F., Talia, M., Tasca, L. A. M., Riechers, D. A., Rodighiero, G., Romano, M., Scoville, N., Toft, S., Vallini, L., Vergani, D., Zamorani, G., and Zucca, E. (2020). The ALPINE-ALMA [C II] Survey: Multiwavelength Ancillary Data and Basic Physical Measurements. *ApJS*, 247(2):61.

Förster Schreiber, N. M., Genzel, R., Bouché, N., Cresci, G., Davies, R., Buschkamp, P., Shapiro, K., Tacconi, L. J., Hicks, E. K. S., Genel, S., Shapley,

A. E., Erb, D. K., Steidel, C. C., Lutz, D., Eisenhauer, F., Gillessen, S., Sternberg, A., Renzini, A., Cimatti, A., Daddi, E., Kurk, J., Lilly, S., Kong, X., Lehnert, M. D., Nesvadba, N., Verma, A., McCracken, H., Arimoto, N., Mignoli, M., and Onodera, M. (2009). The SINS Survey: SINFONI Integral Field Spectroscopy of z ~2 Star-forming Galaxies. *ApJ*, 706(2):1364–1428.

Förster Schreiber, N. M., Genzel, R., Lehnert, M. D., Bouché, N., Verma, A., Erb, D. K., Shapley, A. E., Steidel, C. C., Davies, R., Lutz, D., Nesvadba, N., Tacconi, L. J., Eisenhauer, F., Abuter, R., Gilbert, A., Gillessen, S., and Sternberg, A. (2006). SINFONI Integral Field Spectroscopy of z ~2 UV-selected Galaxies: Rotation Curves and Dynamical Evolution. *ApJ*, 645(2):1062–1075.

Förster Schreiber, N. M. and Wuyts, S. (2020). Star-Forming Galaxies at Cosmic Noon. *ARA&A*, 58:661–725.

Fudamoto, Y., Oesch, P. A., Faisst, A., Béthermin, M., Ginolfi, M., Khusanova, Y., Loiacono, F., Le Fèvre, O., Capak, P., Schaerer, D., Silverman, J. D., Cassata, P., Yan, L., Amorin, R., Bardelli, S., Boquien, M., Cimatti, A., Dessauges-Zavadsky, M., Fujimoto, S., Gruppioni, C., Hathi, N. P., Ibar, E., Jones, G. C., Koekemoer, A. M., Lagache, G., Lemaux, B. C., Maiolino, R., Narayanan, D., Pozzi, F., Riechers, D. A., Rodighiero, G., Talia, M., Toft, S., Vallini, L., Vergani, D., Zamorani, G., and Zucca, E. (2020). The ALPINE-ALMA [CII] survey. Dust attenuation properties and obscured star formation at z $\sim$ 4.4-5.8. *A&A*, 643:A4.

Fujimoto, S., Silverman, J. D., Bethermin, M., Ginolfi, M., Jones, G. C., Le Fèvre, O., Dessauges-Zavadsky, M., Rujopakarn, W., Faisst, A. L., Fudamoto, Y., Cassata, P., Morselli, L., Maiolino, R., Schaerer, D., Capak, P., Yan, L., Vallini, L., Toft, S., Loiacono, F., Zamorani, G., Talia, M., Narayanan, D., Hathi, N. P., Lemaux, B. C., Boquien, M., Amorin, R., Ibar, E., Koekemoer, A. M., Méndez-Hernández, H., Bardelli, S., Vergani, D., Zucca, E., Romano, M., and Cimatti, A. (2020). The ALPINE-ALMA [C II] Survey: Size of Individual Star-forming Galaxies at z = 4-6 and Their Extended Halo Structure. *ApJ*, 900(1):1.

Genzel, R., Tacconi, L. J., Eisenhauer, F., Förster Schreiber, N. M., Cimatti, A., Daddi, E., Bouché, N., Davies, R., Lehnert, M. D., Lutz, D., Nesvadba, N., Verma, A., Abuter, R., Shapiro, K., Sternberg, A., Renzini, A., Kong, X., Arimoto, N., and Mignoli, M. (2006). The rapid formation of a large rotating disk galaxy three billion years after the Big Bang. , 442(7104):786–789.

Ginolfi, M., Jones, G. C., Béthermin, M., Fudamoto, Y., Loiacono, F., Fujimoto, S., Le Févre, O., Faisst, A., Schaerer, D., Cassata, P., Silverman, J. D., Yan, L., Capak, P., Bardelli, S., Boquien, M., Carraro, R., Dessauges-Zavadsky, M., Giavalisco, M., Gruppioni, C., Ibar, E., Khusanova, Y., Lemaux, B. C., Maiolino, R., Narayanan, D., Oesch, P., Pozzi, F., Rodighiero, G., Talia, M., Toft, S., Vallini, L., Vergani, D., and Zamorani, G. (2020). The ALPINE-ALMA

[C II] survey: Star-formation-driven outflows and circumgalactic enrichment in the early Universe. *A&A*, 633:A90.

Graciá-Carpio, J., Sturm, E., Hailey-Dunsheath, S., Fischer, J., Contursi, A., Poglitsch, A., Genzel, R., González-Alfonso, E., Sternberg, A., Verma, A., Christopher, N., Davies, R., Feuchtgruber, H., de Jong, J. A., Lutz, D., and Tacconi, L. J. (2011). Far-infrared Line Deficits in Galaxies with Extreme L_{FIR}/M_{H_{2}} Ratios. *ApJ*, 728(1):L7.

Guilloteau, S. and Lucas, R. (2000). Imaging at the IRAM Plateau de Bure Interferometer. In Mangum, J. G. and Radford, S. J. E., editors, *Imaging at Radio through Submillimeter Wavelengths*, volume 217 of *Astronomical Society of the Pacific Conference Series*, page 299.

Harikane, Y., Ono, Y., Ouchi, M., Liu, C., Sawicki, M., Shibuya, T., Behroozi, P. S., He, W., Shimasaku, K., Arnouts, S., Coupon, J., Fujimoto, S., Gwyn, S., Huang, J., Inoue, A. K., Kashikawa, N., Komiyama, Y., Matsuoka, Y., and Willott, C. J. (2022). GOLDRUSH. IV. Luminosity Functions and Clustering Revealed with 4,000,000 Galaxies at z 2-7: Galaxy-AGN Transition, Star Formation Efficiency, and Implication for Evolution at z $>$ 10. *ApJS*, 259(1):20.

Hashimoto, T., Inoue, A. K., Mawatari, K., Tamura, Y., Matsuo, H., Furusawa, H., Harikane, Y., Shibuya, T., Knudsen, K. K., Kohno, K., Ono, Y., Zackrisson, E., Okamoto, T., Kashikawa, N., Oesch, P. A., Ouchi, M., Ota, K., Shimizu, I., Taniguchi, Y., Umehata, H., and Watson, D. (2019). Big Three Dragons: A z = 7.15 Lyman-break galaxy detected in [O III] 88 μm, [C II] 158 μm, and dust continuum with ALMA. , 71(4):71.

Hashimoto, T., Verhamme, A., Ouchi, M., Shimasaku, K., Schaerer, D., Nakajima, K., Shibuya, T., Rauch, M., Ono, Y., and Goto, R. (2015). A Close Comparison between Observed and Modeled Lyα Lines for z ~2.2 Lyα Emitters. *ApJ*, 812(2):157.

Herrera-Camus, R., Bolatto, A. D., Wolfire, M. G., Smith, J. D., Croxall, K. V., Kennicutt, R. C., Calzetti, D., Helou, G., Walter, F., Leroy, A. K., Draine, B., Brandl, B. R., Armus, L., Sandstrom, K. M., Dale, D. A., Aniano, G., Meidt, S. E., Boquien, M., Hunt, L. K., Galametz, M., Tabatabaei, F. S., Murphy, E. J., Appleton, P., Roussel, H., Engelbracht, C., and Beirao, P. (2015). [C II] 158 μm Emission as a Star Formation Tracer. *ApJ*, 800(1):1.

Herrera-Camus, R., Förster Schreiber, N. M., Price, S. H., Übler, H., Bolatto, A. D., Davies, R. L., Fisher, D., Genzel, R., Lutz, D., Naab, T., Nestor, A., Shimizu, T., Sternberg, A., Tacconi, L., and Tadaki, K. (2022). Kiloparsec view of a typical star-forming galaxy when the Universe was ∼1 Gyr old. II. Regular rotating disk and evidence for baryon dominance on galactic scales. *A&A*, 665:L8.

Herrera-Camus, R., González-López, J., Förster Schreiber, N., Aravena, M., de Looze, I., Spilker, J., Tadaki, K., Barcos-Muñoz, L., Assef, R. J., Birkin, J. E.,

Bolatto, A. D., Bouwens, R., Bovino, S., Bowler, R. A. A., Calistro Rivera, G., da Cunha, E., Davies, R. I., Davies, R. L., Díaz-Santos, T., Ferrara, A., Fisher, D., Genzel, R., Hodge, J., Ikeda, R., Killi, M., Lee, L., Li, Y., Li, J., Liu, D., Lutz, D., Mitsuhashi, I., Narayanan, D., Naab, T., Palla, M., Price, S. H., Posses, A., Relaño, M., Smit, R., Solimano, M., Sternberg, A., Tacconi, L., Telikova, K., Übler, H., van der Giessen, S. A., Veilleux, S., Villanueva, V., and Baeza-Garay, M. (2025). The ALMA-CRISTAL survey: Gas, dust, and stars in star-forming galaxies when the Universe was ~1 Gyr old I. Survey overview and case studies. *arXiv e-prints*, page arXiv:2505.06340.

Herrera-Camus, R., Sturm, E., Graciá-Carpio, J., Lutz, D., Contursi, A., Veilleux, S., Fischer, J., González-Alfonso, E., Poglitsch, A., Tacconi, L., Genzel, R., Maiolino, R., Sternberg, A., Davies, R., and Verma, A. (2018a). SHINING, A Survey of Far-infrared Lines in Nearby Galaxies. I. Survey Description, Observational Trends, and Line Diagnostics. *ApJ*, 861(2):94.

Herrera-Camus, R., Sturm, E., Graciá-Carpio, J., Lutz, D., Contursi, A., Veilleux, S., Fischer, J., González-Alfonso, E., Poglitsch, A., Tacconi, L., Genzel, R., Maiolino, R., Sternberg, A., Davies, R., and Verma, A. (2018b). SHINING, A Survey of Far-infrared Lines in Nearby Galaxies. II. Line-deficit Models, AGN Impact, [C II]-SFR Scaling Relations, and Mass-Metallicity Relation in (U)LIRGs. *ApJ*, 861(2):95.

Hopkins, A. M. and Beacom, J. F. (2006). On the Normalization of the Cosmic Star Formation History. *ApJ*, 651(1):142–154.

Ikeda, R., Tadaki, K.-i., Mitsuhashi, I., Aravena, M., De Looze, I., Förster Schreiber, N. M., González-López, J., Herrera-Camus, R., Spilker, J., Barcos-Muñoz, L., da Cunha, E., Davies, R., Díaz-Santos, T., Ferrara, A., Killi, M., Lee, L. L., Li, J., Lutz, D., Smit, R., Solimano, M., Telikova, K., Übler, H., Veilleux, S., and Villanueva, V. (2024). The ALMA-CRISTAL Survey: Spatial extent of [CII] line emission in star-forming galaxies at $z = 4 - 6$. *arXiv e-prints*, page arXiv:2408.03374.

Jameson, K. E., Bolatto, A. D., Wolfire, M., Warren, S. R., Herrera-Camus, R., Croxall, K., Pellegrini, E., Smith, J.-D., Rubio, M., Indebetouw, R., Israel, F. P., Meixner, M., Roman-Duval, J., van Loon, J. T., Muller, E., Verdugo, C., Zinnecker, H., and Okada, Y. (2018). First Results from the Herschel and ALMA Spectroscopic Surveys of the SMC: The Relationship between [C II]-bright Gas and CO-bright Gas at Low Metallicity. *ApJ*, 853(2):111.

Johnson, H. L., Harrison, C. M., Swinbank, A. M., Tiley, A. L., Stott, J. P., Bower, R. G., Smail, I., Bunker, A. J., Sobral, D., Turner, O. J., Best, P., Bureau, M., Cirasuolo, M., Jarvis, M. J., Magdis, G., Sharples, R. M., Bland-Hawthorn, J., Catinella, B., Cortese, L., Croom, S. M., Federrath, C., Glazebrook, K., Sweet, S. M., Bryant, J. J., Goodwin, M., Konstantopoulos, I. S., Lawrence, J. S., Medling, A. M., Owers, M. S., and Richards, S. (2018). The KMOS

Redshift One Spectroscopic Survey (KROSS): the origin of disc turbulence in z ≈ 1 star-forming galaxies. *MNRAS*, 474(4):5076–5104.

Kaufman, M. J., Wolfire, M. G., Hollenbach, D. J., and Luhman, M. L. (1999). Far-Infrared and Submillimeter Emission from Galactic and Extragalactic Photodissociation Regions. *ApJ*, 527(2):795–813.

Langer, W. D. and Pineda, J. L. (2015). [C ii] emission from galactic nuclei in the presence of X-rays. *A&A*, 580:A5.

Le Fèvre, O., Béthermin, M., Faisst, A., Jones, G. C., Capak, P., Cassata, P., Silverman, J. D., Schaerer, D., Yan, L., Amorin, R., Bardelli, S., Boquien, M., Cimatti, A., Dessauges-Zavadsky, M., Giavalisco, M., Hathi, N. P., Fudamoto, Y., Fujimoto, S., Ginolfi, M., Gruppioni, C., Hemmati, S., Ibar, E., Koekemoer, A., Khusanova, Y., Lagache, G., Lemaux, B. C., Loiacono, F., Maiolino, R., Mancini, C., Narayanan, D., Morselli, L., Méndez-Hernàndez, H., Oesch, P. A., Pozzi, F., Romano, M., Riechers, D., Scoville, N., Talia, M., Tasca, L. A. M., Thomas, R., Toft, S., Vallini, L., Vergani, D., Walter, F., Zamorani, G., and Zucca, E. (2020). The ALPINE-ALMA [CII] survey. Survey strategy, observations, and sample properties of 118 star-forming galaxies at $4 < z < 6$. *A&A*, 643:A1.

Lee, L. L., Förster Schreiber, N., and Herrera-Camus, R. (2025). The ALMA-CRISTAL survey: Resolved kinematic studies of main sequence star-forming galaxies at 4<z<6. *Astronomy & Astrophysics*.

Li, J., Da Cunha, E., González-López, J., Aravena, M., De Looze, I., Förster Schreiber, N. M., Herrera-Camus, R., Spilker, J., Tadaki, K.-i., Barcos-Munoz, L., Battisti, A. J., Birkin, J. E., Bowler, R. A. A., Davies, R., Díaz-Santos, T., Ferrara, A., Fisher, D. B., Hodge, J., Ikeda, R., Killi, M., Lee, L., Liu, D., Lutz, D., Mitsuhashi, I., Naab, T., Posses, A., Relaño, M., Solimano, M., Übler, H., van der Giessen, S. A., and Villanueva, V. (2024). The ALMA-CRISTAL Survey: Spatially Resolved Star Formation Activity and Dust Content in $4 < z < 6$ Star-forming Galaxies. *ApJ*, 976(1):70.

Lilly, S. J., Le Fevre, O., Hammer, F., and Crampton, D. (1996). The Canada-France Redshift Survey: The Luminosity Density and Star Formation History of the Universe to Z approximately 1. *ApJ*, 460:L1.

Lutz, D., Berta, S., Contursi, A., Förster Schreiber, N. M., Genzel, R., Graciá-Carpio, J., Herrera-Camus, R., Netzer, H., Sturm, E., Tacconi, L. J., Tadaki, K., and Veilleux, S. (2016). The far-infrared emitting region in local galaxies and QSOs: Size and scaling relations. *A&A*, 591:A136.

Madau, P. and Dickinson, M. (2014). Cosmic Star-Formation History. *ARA&A*, 52:415–486.

Malhotra, S., Kaufman, M. J., Hollenbach, D., Helou, G., Rubin, R. H., Brauher, J., Dale, D., Lu, N. Y., Lord, S., Stacey, G., Contursi, A., Hunter, D. A., and

Dinerstein, H. (2001). Far-Infrared Spectroscopy of Normal Galaxies: Physical Conditions in the Interstellar Medium. *ApJ*, 561(2):766–786.

Matsuoka, Y., Iwasawa, K., Onoue, M., Kashikawa, N., Strauss, M. A., Lee, C.-H., Imanishi, M., Nagao, T., Akiyama, M., Asami, N., Bosch, J., Furusawa, H., Goto, T., Gunn, J. E., Harikane, Y., Ikeda, H., Izumi, T., Kawaguchi, T., Kato, N., Kikuta, S., Kohno, K., Komiyama, Y., Koyama, S., Lupton, R. H., Minezaki, T., Miyazaki, S., Murayama, H., Niida, M., Nishizawa, A. J., Noboriguchi, A., Oguri, M., Ono, Y., Ouchi, M., Price, P. A., Sameshima, H., Schulze, A., Silverman, J. D., Sugiyama, N., Tait, P. J., Takada, M., Takata, T., Tanaka, M., Tang, J.-J., Toba, Y., Utsumi, Y., Wang, S.-Y., and Yamashita, T. (2019). Subaru High-z Exploration of Low-luminosity Quasars (SHELLQs). X. Discovery of 35 Quasars and Luminous Galaxies at $5.7 \leq z \leq 7.0$. *ApJ*, 883(2):183.

Matsuoka, Y., Onoue, M., Kashikawa, N., Iwasawa, K., Strauss, M. A., Nagao, T., Imanishi, M., Lee, C.-H., Akiyama, M., Asami, N., Bosch, J., Foucaud, S., Furusawa, H., Goto, T., Gunn, J. E., Harikane, Y., Ikeda, H., Izumi, T., Kawaguchi, T., Kikuta, S., Kohno, K., Komiyama, Y., Lupton, R. H., Minezaki, T., Miyazaki, S., Morokuma, T., Murayama, H., Niida, M., Nishizawa, A. J., Oguri, M., Ono, Y., Ouchi, M., Price, P. A., Sameshima, H., Schulze, A., Shirakata, H., Silverman, J. D., Sugiyama, N., Tait, P. J., Takada, M., Takata, T., Tanaka, M., Tang, J.-J., Toba, Y., Utsumi, Y., and Wang, S.-Y. (2018). Subaru High-z Exploration of Low-Luminosity Quasars (SHELLQs). II. Discovery of 32 quasars and luminous galaxies at $5.7 < z \leq 6.8$. , 70:S35.

Mitsuhashi, I., Tadaki, K.-i., Ikeda, R., Herrera-Camus, R., Aravena, M., De Looze, I., Förster Schreiber, N. M., González-López, J., Spilker, J., Assef, R. J., Bouwens, R., Barcos-Munoz, L., Birkin, J., Bowler, R. A. A., Rivera, G. C., Davies, R., Da Cunha, E., Díaz-Santos, T., Ferrara, A., Fisher, D. B., Lee, L. L., Li, J., Lutz, D., Relaño, M., Naab, T., Palla, M., Posses, A., Solimano, M., Tacconi, L., Übler, H., van der Giessen, S., and Veilleux, S. (2024). The ALMA-CRISTAL survey: Widespread dust-obscured star formation in typical star-forming galaxies at $z = 4$–6. *A&A*, 690:A197.

Moutard, T., Sawicki, M., Arnouts, S., Golob, A., Coupon, J., Ilbert, O., Yang, X., and Gwyn, S. (2020). UV and U-band luminosity functions from CLAUDS and HSC-SSP - I. Using four million galaxies to simultaneously constrain the very faint and bright regimes to $z \sim 3$. *MNRAS*, 494(2):1894–1918.

Murphy, E. J., Condon, J. J., Schinnerer, E., Kennicutt, R. C., Calzetti, D., Armus, L., Helou, G., Turner, J. L., Aniano, G., Beirão, P., Bolatto, A. D., Brandl, B. R., Croxall, K. V., Dale, D. A., Donovan Meyer, J. L., Draine, B. T., Engelbracht, C., Hunt, L. K., Hao, C. N., Koda, J., Roussel, H., Skibba, R., and Smith, J. D. T. (2011). Calibrating Extinction-free Star Formation Rate Diagnostics with 33 GHz Free-free Emission in NGC 6946. *ApJ*, 737(2):67.

Narayanan, D. and Krumholz, M. R. (2017). A physical model for the [C II]-FIR deficit in luminous galaxies. *MNRAS*, 467(1):50–67.

Rowland, L. E., Hodge, J., Bouwens, R., Mancera Piña, P. E., Hygate, A., Algera, H., Aravena, M., Bowler, R., da Cunha, E., Dayal, P., Ferrara, A., Herard-Demanche, T., Inami, H., van Leeuwen, I., de Looze, I., Oesch, P., Pallottini, A., Phillips, S., Rybak, M., Schouws, S., Smit, R., Sommovigo, L., Stefanon, M., and van der Werf, P. (2024). REBELS-25: discovery of a dynamically cold disc galaxy at z = 7.31. *MNRAS*, 535(3):2068–2091.

Schaerer, D., Ginolfi, M., Béthermin, M., Fudamoto, Y., Oesch, P. A., Le Fèvre, O., Faisst, A., Capak, P., Cassata, P., Silverman, J. D., Yan, L., Jones, G. C., Amorin, R., Bardelli, S., Boquien, M., Cimatti, A., Dessauges-Zavadsky, M., Giavalisco, M., Hathi, N. P., Fujimoto, S., Ibar, E., Koekemoer, A., Lagache, G., Lemaux, B. C., Loiacono, F., Maiolino, R., Narayanan, D., Morselli, L., Méndez-Hernàndez, H., Pozzi, F., Riechers, D., Talia, M., Toft, S., Vallini, L., Vergani, D., Zamorani, G., and Zucca, E. (2020). The ALPINE-ALMA [C II] survey. Little to no evolution in the [C II]-SFR relation over the last 13 Gyr. *A&A*, 643:A3.

Simons, R. C., Kassin, S. A., Weiner, B. J., Faber, S. M., Trump, J. R., Heckman, T. M., Koo, D. C., Pacifici, C., Primack, J. R., Snyder, G. F., and de la Vega, A. (2017). z $\sim$ 2: An Epoch of Disk Assembly. *ApJ*, 843(1):46.

Smith, J. D. T., Croxall, K., Draine, B., De Looze, I., Sandstrom, K., Armus, L., Beirão, P., Bolatto, A., Boquien, M., Brandl, B., Crocker, A., Dale, D. A., Galametz, M., Groves, B., Helou, G., Herrera-Camus, R., Hunt, L., Kennicutt, R., Walter, F., and Wolfire, M. (2017). The Spatially Resolved [CII] Cooling Line Deficit in Galaxies. *ApJ*, 834(1):5.

Spilker, J. S., Marrone, D. P., Aravena, M., Béthermin, M., Bothwell, M. S., Carlstrom, J. E., Chapman, S. C., Crawford, T. M., de Breuck, C., Fassnacht, C. D., Gonzalez, A. H., Greve, T. R., Hezaveh, Y., Litke, K., Ma, J., Malkan, M., Rotermund, K. M., Strandet, M., Vieira, J. D., Weiss, A., and Welikala, N. (2016). ALMA Imaging and Gravitational Lens Models of South Pole Telescope—Selected Dusty, Star-Forming Galaxies at High Redshifts. *ApJ*, 826(2):112.

Steidel, C. C., Erb, D. K., Shapley, A. E., Pettini, M., Reddy, N., Bogosavljević, M., Rudie, G. C., and Rakic, O. (2010). The Structure and Kinematics of the Circumgalactic Medium from Far-ultraviolet Spectra of z ~= 2-3 Galaxies. *ApJ*, 717(1):289–322.

Stott, J. P., Swinbank, A. M., Johnson, H. L., Tiley, A., Magdis, G., Bower, R., Bunker, A. J., Bureau, M., Harrison, C. M., Jarvis, M. J., Sharples, R., Smail, I., Sobral, D., Best, P., and Cirasuolo, M. (2016). The KMOS Redshift One Spectroscopic Survey (KROSS): dynamical properties, gas and dark matter fractions of typical z $\sim$ 1 star-forming galaxies. *MNRAS*, 457(2):1888–1904.

Übler, H., Genzel, R., Wisnioski, E., Förster Schreiber, N. M., Shimizu, T. T., Price, S. H., Tacconi, L. J., Belli, S., Wilman, D. J., Fossati, M., Mendel, J. T., Davies, R. L., Beifiori, A., Bender, R., Brammer, G. B., Burkert, A., Chan, J., Davies, R. I., Fabricius, M., Galametz, A., Herrera-Camus, R., Lang, P., Lutz, D., Momcheva, I. G., Naab, T., Nelson, E. J., Saglia, R. P., Tadaki, K., van Dokkum, P. G., and Wuyts, S. (2019). The Evolution and Origin of Ionized Gas Velocity Dispersion from z $\sim$ 2.6 to z $\sim$ 0.6 with KMOS^{3D}. *ApJ*, 880(1):48.

Verhamme, A., Schaerer, D., and Maselli, A. (2006). 3D Lyα radiation transfer. I. Understanding Lyα line profile morphologies. *A&A*, 460(2):397–413.

Wisnioski, E., Förster Schreiber, N. M., Fossati, M., Mendel, J. T., Wilman, D., Genzel, R., Bender, R., Wuyts, S., Davies, R. L., Übler, H., Bandara, K., Beifiori, A., Belli, S., Brammer, G., Chan, J., Davies, R. I., Fabricius, M., Galametz, A., Lang, P., Lutz, D., Nelson, E. J., Momcheva, I., Price, S., Rosario, D., Saglia, R., Seitz, S., Shimizu, T., Tacconi, L. J., Tadaki, K., van Dokkum, P. G., and Wuyts, E. (2019). The KMOS^{3D} Survey: Data Release and Final Survey Paper. *ApJ*, 886(2):124.

Wisnioski, E., Förster Schreiber, N. M., Wuyts, S., Wuyts, E., Bandara, K., Wilman, D., Genzel, R., Bender, R., Davies, R., Fossati, M., Lang, P., Mendel, J. T., Beifiori, A., Brammer, G., Chan, J., Fabricius, M., Fudamoto, Y., Kulkarni, S., Kurk, J., Lutz, D., Nelson, E. J., Momcheva, I., Rosario, D., Saglia, R., Seitz, S., Tacconi, L. J., and van Dokkum, P. G. (2015). The KMOS^{3D} Survey: Design, First Results, and the Evolution of Galaxy Kinematics from 0.7 <= z <= 2.7. *ApJ*, 799(2):209.

Wolfire, M. G., Hollenbach, D., and McKee, C. F. (2010). The Dark Molecular Gas. *ApJ*, 716(2):1191–1207.

Wolfire, M. G., McKee, C. F., Hollenbach, D., and Tielens, A. G. G. M. (2003). Neutral Atomic Phases of the Interstellar Medium in the Galaxy. *ApJ*, 587(1):278–311.

Wuyts, S., Labbé, I., Förster Schreiber, N. M., Franx, M., Rudnick, G., Brammer, G. B., and van Dokkum, P. G. (2008). FIREWORKS U_{38}-to-24 μm Photometry of the GOODS Chandra Deep Field-South: Multiwavelength Catalog and Total Infrared Properties of Distant K_s-selected Galaxies. *ApJ*, 682(2):985–1003.

Zavala, J. A., Casey, C. M., Manning, S. M., Aravena, M., Bethermin, M., Caputi, K. I., Clements, D. L., Cunha, E. d., Drew, P., Finkelstein, S. L., Fujimoto, S., Hayward, C., Hodge, J., Kartaltepe, J. S., Knudsen, K., Koekemoer, A. M., Long, A. S., Magdis, G. E., Man, A. W. S., Popping, G., Sanders, D., Scoville, N., Sheth, K., Staguhn, J., Toft, S., Treister, E., Vieira, J. D., and Yun, M. S. (2021). The Evolution of the IR Luminosity Function and Dust-obscured Star Formation over the Past 13 Billion Years. *ApJ*, 909(2):165.